



# Investigation of Decaying $\beta$ -Configuration Sunspot in Active Region NOAA 13229

Shahid Idrees<sup>1,2</sup> · Jiangtao Su<sup>1,2</sup> · Jie Chen<sup>1,2</sup> · Yuanyong Deng<sup>1,2</sup>

Received: 5 December 2023 / Accepted: 13 May 2024 / Published online: 24 June 2024  
© The Author(s), under exclusive licence to Springer Nature B.V. 2024

## Abstract

In this study, we investigate the decay of sunspots in the active region NOAA 13229 using data from the ASO-S/FMG and SDO/HMI. We closely examine the decay patterns of sunspots S1 and S2, which reveal different decay rates and features due to the mechanisms of magnetic cancellation, dispersion, and the role of horizontal flows. Our analysis highlights the significant impact of magnetic flux changes, including the decrease of both the sunspot area and magnetic flux over time, which adheres to distinct decay laws. This study elucidates the complex interplay between magnetic submergence, cancellation, and dispersion in the sunspot decay process, contributing to our understanding of the underlying mechanisms driving these phenomena. Our results emphasize the importance of horizontal flow dynamics in shaping the decay characteristics of sunspots, providing insights for the role played by the magnetic and plasma processes in solar active regions.

**Keywords** Sunspots · Solar activity · Solar flares · Active regions

## 1. Introduction

Sunspot study is an important and hot topic of research in solar physics due to some main reasons: (i) sunspots have a significant impact on the Sun's magnetic field, (ii) sunspots are the major source of solar activity such as CMEs, solar flares, etc., (iii) sunspots may be utilized to investigate the underlying structure and dynamics of the Sun. Sunspots are the most essential feature of the photosphere, consisting of the umbra and penumbra. The difference between a sunspot and a pore is the presence of penumbra. A lot of research

---

✉ S. Idrees  
[shahidbsp1341@gmail.com](mailto:shahidbsp1341@gmail.com)

✉ J. Su  
[slt@bao.ac.cn](mailto:slt@bao.ac.cn)

J. Chen  
[chenjie@bao.ac.cn](mailto:chenjie@bao.ac.cn)

Y. Deng  
[dyy@nao.cas.cn](mailto:dyy@nao.cas.cn)

<sup>1</sup> University of Chinese Academy of Sciences, Beijing 100049, China

<sup>2</sup> National Astronomical Observatories, Chinese Academy of Sciences, Beijing 100012, China

has been conducted from a simulation and observation perspective towards the generation of sunspot penumbra (Leka and Skumanich, 1998; Schlichenmaier et al., 2010; Romano et al., 2020; Li et al., 2018; Murabito et al., 2016; Romano et al., 2014; Lim et al., 2013; Shimizu, Ichimoto, and Suematsu, 2012; Rempel, 2011, 2012; MacTaggart, Guglielmino, and Zuccarello, 2016; Thomas et al., 2002). On the other hand, the process behind sunspot decay is still poorly understood.

Sunspot decay can be studied from two perspectives. One of them is the study of the area decay of sunspots, termed photometric decay. The other is the study of the process of diminished magnetic flux from the photosphere, known as magnetic flux diffusion. It was studied by Bumba (1963) who observed that the area of the sunspot declines linearly with respect to time. He also made significant contributions by studying the decay rates of leader and follower sunspots. Different decay laws have been proposed by previous studies related to sunspot decay, like linear decay law (Martinez Pillet, Moreno-Insertis, and Vazquez, 1993; Rüdiger and Kitchatinov, 2000; Chapman et al., 2003; Gafeira et al., 2014; Muraközy, 2020), parabolic decay law (Litvinenko and Wheatland, 2015; Petrovay and van Driel-Gesztelyi, 1997; Petrovay, Martínez Pillet, and van Driel-Gesztelyi, 1999), quadratic decay law, exponential decay law, etc. Solanki (2003) proposed that 95% of sunspot decay follows the linear decay law.

The decay mechanisms responsible for the linear and parabolic decay laws of the sunspot area are likely to be distinct. Meyer et al. (1974) proposed a model to explain the linear decay law, attributing it to turbulent magnetic diffusion within a sunspot. This turbulent diffusion model suggests that the loss of magnetic flux within the sunspot occurs uniformly throughout its entire area, regardless of the sunspot size or perimeter length (Krause and Ruediger, 1975; Martínez Pillet, 2002). In contrast, the parabolic decay law is more consistent with the turbulent erosion model. According to this model, the decay of a sunspot is primarily driven by the erosion of its outer boundary. In other words, the decay rate is expected to be directly proportional to the length of the sunspot perimeter (Petrovay and van Driel-Gesztelyi, 1997; Petrovay and Moreno-Insertis, 1997; Martínez Pillet, 2002; Solanki, 2003; Litvinenko and Wheatland, 2015).

In addition to the decay of sunspot area, the decay of magnetic flux is a significant process during the decay of sunspots. Skumanich and Lites (1994) observed a linear decrease in the total magnetic flux of symmetric sunspots over time, with a decay rate of  $0.9 \times 10^{20}$  Mx day<sup>-1</sup>. Verma and Denker (2012) conducted a study on active region NOAA 11126 using the Helioseismic and Magnetic Imager (HMI) and reported decay rates of 2.3 and  $4.7 \times 10^{20}$  Mx day<sup>-1</sup> for the positive and negative magnetic fluxes, respectively. Similarly, Sheeley et al. (2017) analyzed 36 sunspots using HMI magnetograms and continuum images, finding a nearly linear decreasing trend in the magnetic fluxes of certain sunspots, with an average decay rate of  $2-4 \times 10^{20}$  Mx day<sup>-1</sup>. Rempel (2015) performed simulations of a sunspot and observed a linear decay of magnetic flux within its umbra. The decay rate increases linearly with group size until a certain point, beyond which it stabilizes. The decay rate per individual sunspot indicates a diffusion process. Variations in decay rates are noted across latitudes, with limited evidence for differences between solar cycles (Hathaway and Choudhary, 2008).

Among the most significant observational evidence of sunspot decay are moving magnetic features (MMFs). It has been always considered that MMFs are the cause of magnetic flux transfer from a sunspot during sunspot decay (Chen et al., 2015). As a result of an interplay between the Evershed flow, moat flows, and penumbra magnetic field, MMFs are produced during the sunspot decay (Martínez Pillet, 2002). There is a strong relation between the Evershed flows, moat flows, and MMFs (Cabrera Solana et al., 2006; Sainz Dalda

and Martínez Pillet, 2005). Deng et al. (2007) suggested that the magnetic flux removal is preceded by three steps: breaking up of the umbra, flux cancellation of MMFs, and dispersion of flux via MMFs. Verma and Denker (2012) studied MMFs as the main reason for magnetic flux removal and they also noticed the horizontal flows in the vicinity of sunspots during sunspot decay. Afterwards, horizontal flow fields have been observed by using HMI Doppler maps (Strecker and Bello González, 2018). Moat flow has been found around the decaying sunspots whose velocity decreased with the decay of sunspots. In addition, various studies have suggested that in the phase of sunspot decay the horizontal magnetic fields within the penumbra undergo a transformation, becoming vertical (Bellot Rubio, Tritschler, and Martínez Pillet, 2008; Watanabe, Kitai, and Otsuji, 2014; Verma et al., 2018)). As these penumbral magnetic fields rise towards the chromosphere due to buoyancy, the penumbra of the sunspot gradually diminishes in the photosphere. Similarly, the rapid fading of the penumbra after a solar flare is attributed to the rearrangement of the magnetic field lines (Wang et al., 2004; Deng et al., 2005)). In simulations conducted by Rempel (2015), it was observed that the submergence of a magnetic field played a significant role in sunspot decay. However, due to challenges linked to observing flow motions beneath the photosphere, there is currently no evidence to support this perspective.

Previous research into the decay of sunspots has primarily focused on configurations of sunspots with attention given to the decay process of individual configurations. To highlight this gap, we conducted a study specifically examining the decay phase of  $\beta$ -configuration sunspots. We closely analyzed two sunspots (S1 and S2) during their decay stage. For an account of our observations and methods used in this study, please refer to Section 2. The implications of our gathered data and subsequent discussions are presented in Section 3. Finally, we outline the conclusions drawn from our findings in Section 4.

## 2. Method and Observation

The focus of our observational study is the decay of sunspots in the active region (AR) NOAA 13229 which occurred from 00:01 UT on 2023 February 22 to 17:06 UT on 2023 February 25. The decay of a specified sunspot is interesting because it relates to four flares occurring during its decay period (Shimizu, Ichimoto, and Suematsu, 2012). Data has been taken from the ASO-S (Advanced Space-based Solar Observatory) and SDO (Solar Dynamics Observatory). The ASO-S (Chinese nickname Kuafu-1) is the first Chinese comprehensive dedicated solar observatory in space (Gan et al., 2019, 2023). Its primary scientific objective is to improve our understanding of a variety of solar phenomena such as solar flares, CMEs, solar magnetic field, and their relationships. In addition, it has consequences for understanding the dynamics of the Sun and its impact on space weather. The Full-disk vector MagnetoGraph (Deng et al., 2019) on board the ASO-S is designed to measure the photospheric magnetic fields over the entire solar disk through Fe I 532.42 nm line with high spatial and temporal resolutions, and high magnetic sensitivity. The Full-disk MagnetoGraph (FMG) boasts a 14-cm aperture and a high-resolution  $4096 \times 4096$  pixel CMOS camera. FMG observes polarized Stokes images using a Liquid Crystal Variable Retarder (Hou et al., 2020). FMG measures longitudinal magnetic fields with a sensitivity of 15 G in the normal mode. Temporal resolution varies, offering 30-second updates for single-component magnetograms and 2-minute intervals for vector magnetogram acquisition in normal mode. Spatially, the instrument achieves roughly 1.5 arcseconds resolution with a 0.55 arcsecond pixel size (Deng et al., 2019; Su et al., 2019), further enhanced to 1.04 arcseconds for the

flight model (Gan et al., 2023). These specifications highlight the FMG's powerful capabilities in unraveling the intricate tapestry of the Sun's magnetic landscape. Here we utilized the photospheric line-of-sight (LOS) magnetograms and continuum intensitygrams taken by the ASO-S/FMG. The Solar Dynamics Observatory (SDO) was launched by NASA in 2010 as a space probe. It holds the pioneer spacecraft exclusively designed to observe the Sun across several wavelengths at the time. The Helioseismic and Magnetic Imager (HMI) is one of the instruments carried by the SDO and it routinely measures photospheric velocity and magnetic field of the Sun. The HMI instrument (Schou et al., 2012) on board SDO obtains full solar disk images in the photospheric absorption line Fe I centered at the wavelength of 6173.3 Å which has two cameras with spatial and temporal resolution of 0.5'' per pixel and 45 seconds, respectively. It measures Doppler velocity, line-of-sight magnetic fields, and vector magnetic fields in the solar photosphere (Liu et al., 2012). An inversion method is then used to construct the vector magnetic field by inverting the Stokes parameters. HMI vector magnetic field data boasts an impressive spatial resolution of 0.5'' (Jiang and Feng, 2013), allowing scientists to discern intricate details of the Sun's magnetic field. Additionally, the data is captured with a cadence of 12 minutes, providing frequent updates on the Sun's ever-changing magnetism. The HMI data is utilized to study the different features like sunspots, solar flares, CMEs, etc. It is also used to develop models to study the interior and atmosphere of the Sun (Hoeksema and HMI Project Team, 2007; Scherrer et al., 2012; Démoulin and Berger, 2003).

The data has been analyzed by applying different operations like rotation, shifting, map creation, etc. To remove the solar differential rotation, the *drot\_map.pro* function in SSW is applied on both the FMG full-disk Stokes V data and HMI longitudinal magnetic field with respect to the reference time, 2023 February 22, 17:00:00. We then cut out the related active region (NOAA 13229) in FMG time-series images (FOV of 500 arcsec  $\times$  400 arcsec). The FMG Stokes V images taken at different times are calibrated based on the linear calibration in the weak-field approximation defined by the differential solar rotation (Su et al., 2019). We obtained the flow maps by using the local cross-correlation tracking method (November and Simon, 1988; Chae, 2001) which describes the flow pattern of horizontal flows through sunspots and in the vicinity of sunspots. The Local Cross-correlation Tracking (LCT) method is a technique used to determine the horizontal velocities of magnetic field lines at photospheric footpoints. This method involves measuring the local displacements of magnetic flux concentrations between two successive magnetograms using the technique of local correlation tracking. The LCT method is fast and easy to implement, employing the fast Fourier transform to determine the horizontal velocities of magnetic field lines at selected points. The method involves determining the horizontal flow vectors at the centers of macropixels with a size where the absolute value of the magnetic flux density is greater than a certain threshold. The observed flow patterns are evaluated for their physical significance in the transport of magnetic helicity through the solar surface. We took the radial component of the magnetic field for analysis, 8.5'' for the FWHM of the apodizing window and 24 minutes for the time interval  $\Delta t$  between the two frames to be compared. The horizontal velocity (flow) maps were arranged in the time series from 2023 February 22 (00:10 UT) to 2023 February 25 (23:10 UT). These time periods were selected based on significant changes in sunspot morphology and magnetic field configuration, corresponding to the stages of decay as observed in our study. The averaged flow fields for these periods are presented in Figures 5 through 8, showcasing the flow dynamics at crucial intervals: Stage I: Averaged over 2023 February 22, 00:10 UT to 2023 February 23, 05:58 UT; Stage II: Averaged over 2023 February 23, 06:10 UT to 2023 February 23, 15:58 UT; Stage III: Averaged over 2023 February 23, 16:10 UT to 2023 February 24, 22:10 UT; Stage IV: Averaged over 2023 February 24, 22:34 UT to 2023 February 25, 23:10 UT.

The rate at which electromagnetic energy is transmitted from a photosphere to the corona in the presence of horizontal shear or winding motion and a new emerging magnetic flux in the vertical direction is defined as (Démoulin and Berger, 2003)

$$\dot{E} = \iint_{S_p} \frac{1}{\mu_0} (\mathbf{E} \times \mathbf{B}) dS = - \int_{S_p} \frac{B_z}{\mu_0} (\mathbf{v}_t \cdot \mathbf{B}_t) dS + \int_{S_p} \left( \frac{B_t^2}{\mu_0} \right) v_z dS. \quad (1)$$

The first term on the right-hand side represents the energy flow transported by horizontal shear or winding flows, while the second represents the energy flow transported by the new emerging magnetic flux in the vertical direction. The velocity of the tracking magnetic field footpoint motion measurement ( $\mathbf{u}$ ) comes from two contributions,

$$\mathbf{u} = \mathbf{v}_t - \frac{v_z}{B_z} \mathbf{B}_t, \quad (2)$$

where the first term ( $v_t$ ) on the right-hand side shows the horizontal flows and the second (including  $v_z$ ) represents the vertical magnetic flows. Equation 1 can be written as

$$\dot{E} = - \int_{S_p} \frac{B_z}{\mu_0} (\mathbf{u} \cdot \mathbf{B}_t) dS. \quad (3)$$

We used the data from HMI/SDO and the above equations to examine the magnetic fluxes, magnetic energy transport rate, and accumulation energy evolution with respect to time as shown in Figure 3.

AR13229 was classified as a  $\beta$ -type sunspot group, which included the following: sunspot (S1), sunspot (S2) located around the magnetic polarity inverse line, and leading sunspots (S3 and S4). The study offers an understanding that the decay of sunspots (S1 and S2) proceeded due to processes known as submergence of magnetic flux, fragmentation, magnetic cancellation, magnetic diffusion, convergence, and rotation of horizontal flows that contributed to the decay of the sunspots. We also found proof of the existence of the magnetic flux submergence which plays a significant role in sunspot decay. Our observational results (Figure 3) verify the existence of the submergence process of magnetic flux.

### 3. Results

In this section, we discuss the results of our investigation of the decaying  $\beta$ -configuration sunspot in the active region NOAA 13229. The decay process of the  $\beta$ -type sunspot can be seen in Figure 1. The decay of the sunspot area is shown in the left panels (a1, b1, c1, d1) whereas the right panels (a2, b2, c2, d2) of Figure 1 show a pattern of the magnetic flux diminished. The sunspot S1 decayed rapidly from 00:01 UT on 2023 February 22 to 17:06 UT on 2023 February 24. There was only a small pore left at the end. The negative flux in the sunspot S1 was dominant and it was surrounded by a little positive flux. It decreased less significantly compared to the sunspot area in the sunspot S1. So, the magnetic cancellation phenomenon (i.e., when opposite magnetic field polarities encounter and cancel out each other) has not occurred prominently in the sunspot S1 because of a little (negligible) positive flux as compared to the negative flux. In addition, magnetic diffusion and fragmentation processes have been observed in the sunspot S1 which were prominent. Some pores separated from the sunspot S1 are highlighted with blue and red arrows, and a rotation of horizontal flows can be observed by following red arrows in panels b1, c1, and d1.

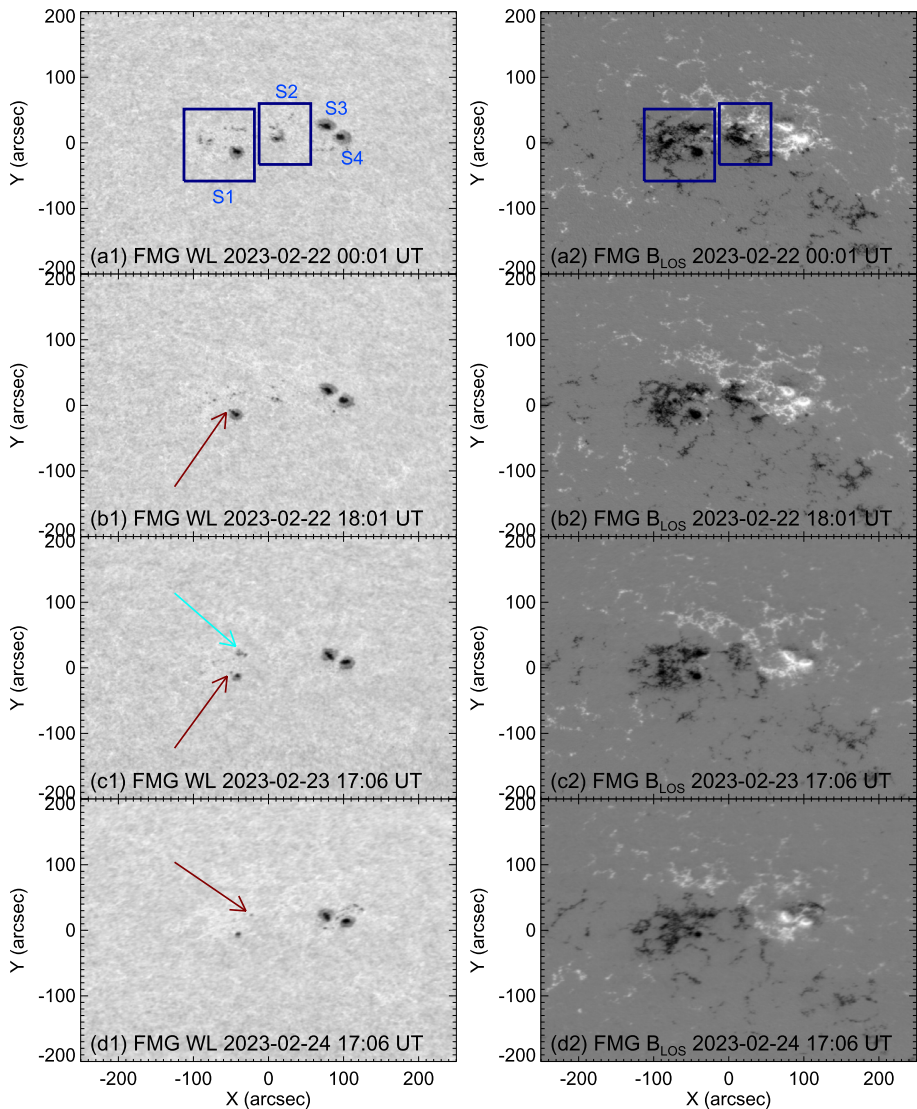


**Figure 1** Left panels (a1, b1, c1, d1) show the area decay pattern of sunspots (focused on S1 and S2) with respect to time. The red arrows indicate the rotation of a separated part and the light blue arrow represents disintegration of a sunspot. Right panels (a2, b2, c2, d2) represent the magnetic flux decay with respect to time. Both rectangles in the panels show the sunspots we focused on (S1 and S2). The map has a field of view of  $500 \text{ arcsec} \times 400 \text{ arcsec}$ .

The sunspot S2 decayed more rapidly from 00:01 UT on 2023 February 22 to 17:06 UT on 2023 February 24. It has completely disappeared at last and nothing remained. The negative flux in the sunspot S2 was surrounded by positive flux on its north and west sides. Both fluxes decreased significantly, which can be observed in the last panel (d2). So, it can be clearly seen that magnetic flux cancellation is dominant in the sunspot S2 compared to the sunspot S1 because the positive flux quantity is comparable to the negative flux so they can

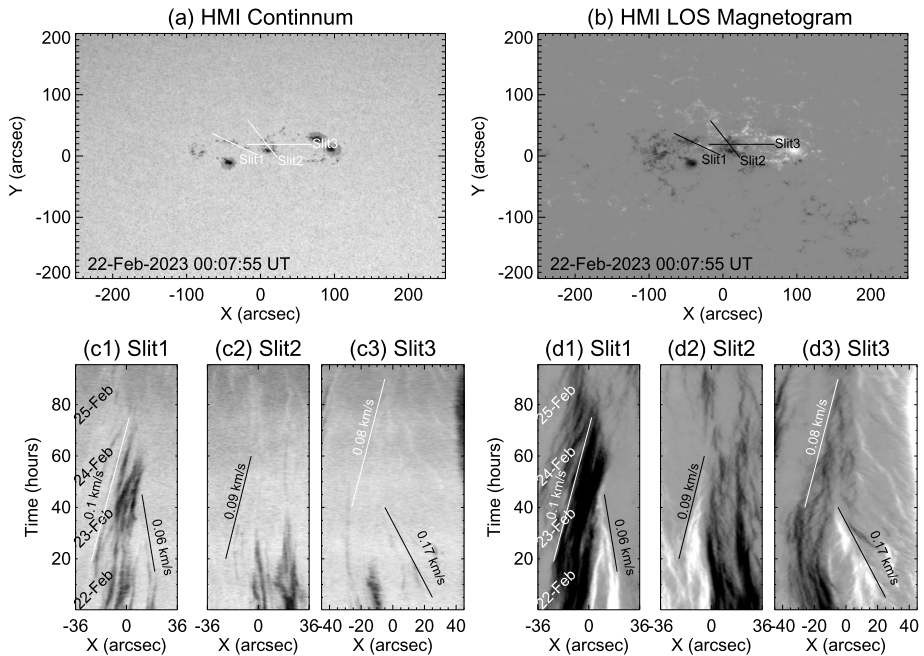
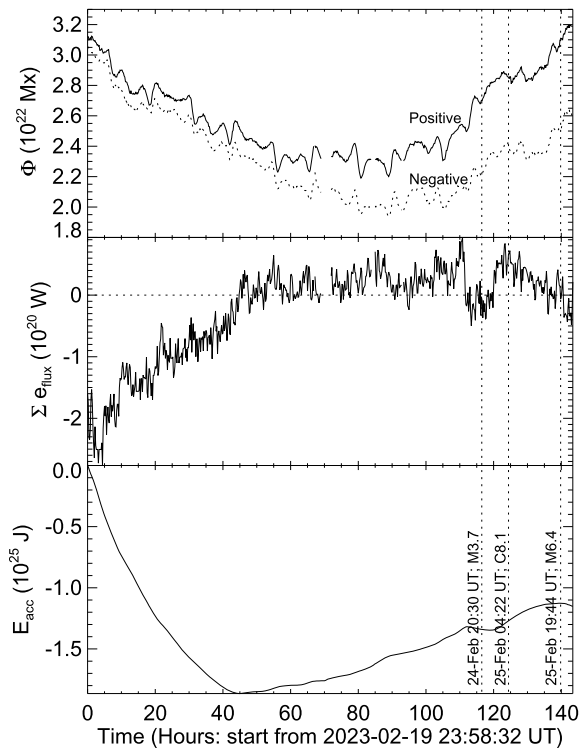


**Figure 2** Top: (a) Three slit positions (slit1, slit2, slit3) drawn on the HMI continuum (b) HMI LOS magnetogram. Bottom: panels c1–c3 and d1–d3 represent the space–time diagrams of magnetic cancellation. Where oblique straight lines are used to calculate the positive and negative flux speeds and these panels are used to verify the magnetic cancellation time up to 50 hours (similar to Figure 3). The map has the field of view of 500 arcsec  $\times$  400 arcsec.

cancel or annihilate each other. This may be the reason why the sunspot S2 decayed more rapidly than the sunspot S1 and the sunspot S2 disappeared completely at the end. Meanwhile, the leading sunspots, S3 and S4, seemed to decay the least, and there were many tiny pores which emerged on their north-west at 17:06 UT on 2023 February 24 (panel d1). To verify the magnetic cancellation, we take three slits marked on the HMI longitudinal magnetogram and continuum as shown in Figure 2 (a and b). They mainly pass through the magnetic cancellation regions (encountering area of positive and negative flux) of the sunspots S1 and S2. In the sunspot S1, the magnetic cancellation (i.e., when opposite magnetic polarity fluxes approach each other, merge, and, as the result of the encounter, magnetic flux decreases due to cancellation of a positive flux concentration by a negative one) occurred in the north-west corner as shown in Figure 1. In sunspot S2, the positive flux surrounded and cancelled the negative flux from its north-western areas. The bottom panels, c1–c3 and d1–d3, show space–time diagrams of magnetic cancellation, which are stacked with slits 1 and 2 taken at different times. The oblique straight line is used to calculate the velocities of positive and negative fluxes as shown in Figure 2 (panels c1, c2, c3, d1, d2, d3).

We analyzed the time evolution of positive and negative magnetic flux, total energy transport from the photosphere to the corona, and energy accumulation in the corona as shown in Figure 3, and found proof for the existence of submergence. The top panel of the figure shows a decrease of positive and negative fluxes which verify the process of cancellation of magnetic fluxes. The middle panel of the figure shows the negative transport rate of magnetic energy from the photosphere to the corona, i.e., there is a net loss of magnetic energy

**Figure 3** Time-dependent evolution of magnetic fluxes, total transport energy, and energy accumulation. The top panel shows the time-dependent variation of positive and negative magnetic fluxes. The middle panel represents the total magnetic energy transport rate from the photosphere to the corona. The bottom panel shows the variation in energy accumulation in corona with respect to time. Here, the time period used for the analysis presented in Figure 4 is highlighted, providing a direct correlation between the observed flux changes and the decay patterns discussed.



transfer in the corona. The bottom panel of the figure shows the loss of energy accumulation in the corona. The negative energy transport from the photosphere to the corona and a decrease in the energy accumulation in the corona may be caused by the submergence of magnetic flux. It can be noticed from Figures 2 and 3 that magnetic cancellation may be closely related to the submergence process because the magnetic cancellation (see Figure 2, y-axis of panels d1–d2), negative transport rate of magnetic energy and accumulation energy loss occurred for almost 50 hours (see top and bottom panels of Figure 3) which may be verified in a future research.

It is also noticed that the shapes of sunspots S3 and S4 transformed from nearly round (panel a1) to oval (panel c1), and their alignment also changed. On the other hand, sunspot S1 transformed from a nearly round shape to an elongated one (panel b1) and then finally converted into a rounded shape (panel d1). The transformation of shapes and alignment of sunspots may be caused by the interaction between the sunspot and surrounding plasma, convective flows in the sunspot, rotation of horizontal flows, differential rotation of Sun, etc. In this paper, we focused only on the decay of two sunspots, S1 and S2.

The decay of sunspot S1 and S2 area ( $\times 10^{14} \text{ m}^2$ ) with respect to time (hours) is shown in Figure 4(a). The decay of the sunspot S1 (blue curve) can be divided into four stages. In the initial stage, it is noticed that the sunspot S1 area decayed faster in the first 30 hours. During the second stage, almost no decay in the area has been observed within the next 10 hours. Meanwhile, in the third stage, fast decay is perceived in the following 30 hours. In the course of the fourth stage, moderate decay has been examined during the last 25 hours. As a result, it is found that the decay curve of the sunspot S1 area followed the parabolic function or pattern. The area of the sunspot S2 (red curve) decayed nearly completely in



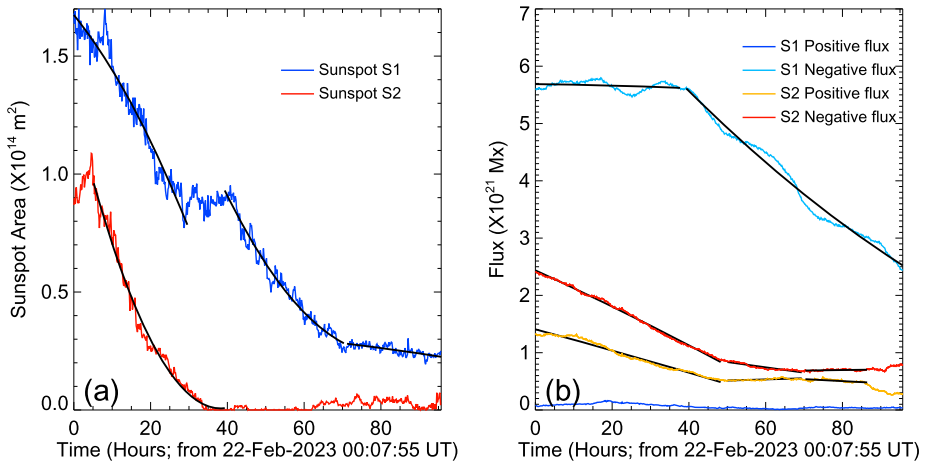


**Figure 4** Panel (a) represents the sunspot area ( $\times 10^{14} \text{ m}^2$ ) decay pattern versus time (hours) for both sunspots S1 (blue) and S2 (red). Panel (b) shows the variation of positive and negative magnetic fluxes ( $\times 10^{21} \text{ Mx}$ ) of both sunspots S1 (dark blue for positive and light blue for negative) and S2 (yellow for positive and red for negative) with respect to time (hours).

35 hours from 05:07 UT on 2023 February 22 to 11:07 UT on 2023 February 23. The sunspot S2 decayed faster compared to the sunspot S1 due to both the more prominent phenomenon of magnetic cancellation (i.e., positive flux is quantitatively comparable to the negative flux) and magnetic diffusion observed in the sunspot S2 and less prominent (like negligible magnetic cancellation) in the sunspot S1. The area decay curve of the sunspot S2 obeyed the exponential decaying function.

In Figure 4(b), it can be noticed that the positive flux of the sunspot S1 (dark blue curve) always remained at a very low level (nearly zero) and can be considered negligible, whereas the change of negative flux of the sunspot S1 (light blue curve) can be divided into two stages. There was a slight change (negligibly small change) in the first 40 hours from 00:07 UT on 2023 February 22 to 16:07 UT on 2023 February 23 and then it decreased linearly in the next 55 hours. In other words, we can say there is no significant magnetic cancellation in the sunspot S1 but magnetic diffusion played an important role in its decay. The negative flux ( $2.4 \times 10^{21} \text{ Mx}$ ) of the sunspot S2 was larger than its positive flux ( $1.3 \times 10^{21} \text{ Mx}$ ) and they decreased linearly in the first 50 hours and nearly kept unchanged in the next 30 hours from 00:07 UT on 2023 February 22 to 08:07 UT on 2023 February 25. However, both positive and negative fluxes have almost the same variation trend with respect to time. Both declined almost at the same rate. As a result, we can say that the magnetic cancellation process occurred significantly in the case of sunspot S2. More detailed information on the sunspots S1 and S2 related to diffusion features, such as diffusion of positive flux, negative flux, and area decay rates during specific time duration, can be found in Tables 1 and 2, respectively.

The flow maps obtained by the LCT technique representing the horizontal velocity via sunspots and in the vicinity of the sunspots are shown in Figure 5. The flows are represented by small arrows whose length represents the strength of flows and arrowheads show the direction of flows. In addition, the red and blue arrows represent the opposite polarities of magnetic flux (represent the horizontal velocity of the magnetic field features). The background of Figure 5(a) is the HMI continuum and that of Figure 5(b) is the HMI longitudinal

**Table 1** Information related to diffusion and decay rate of the sunspot S1.

No.	Time (UT)	Diffusion features	Negative flux decay rate ( $\text{Mx s}^{-1}$ )	Area decay rate or magnetic diffusivity ( $\text{m}^2 \text{s}^{-1}$ )
1	2023-02-22(00:10) to 02-23(23:06:11)	Fast decay without magnetic flux change	$-2.0 \times 10^{14}$	$5.6 \times 10^8$
2	2023-02-23(06:11) to 02-23(16:16)	No decay and no magnetic flux change	$-2.0 \times 10^{14}$	0
3	2023-02-23(16:16) to 02-24(22:29)	Fast decay with flux decrease	$-2.3 \times 10^{16}$	$1.8 \times 10^9$
4	2023-02-24(22:29) to 02-25(23:50)	Slow decay with flux decrease	$-2.3 \times 10^{16}$	$2.8 \times 10^6$

**Table 2** Information related to diffusion and decay rate of the sunspot S2.

No.	Time (UT)	Diffusion features	Positive flux decay rate ( $\text{Mx s}^{-1}$ )	Negative flux decay rate ( $\text{Mx s}^{-1}$ )	Area decay rate or magnetic diffusivity ( $\text{m}^2 \text{s}^{-1}$ )
1	2023-02-22(05:07) to 02-23(23:16:07)	Fast decay with decreasing flux	$-5.0 \times 10^{15}$	$-8.5 \times 10^{15}$	$1.9 \times 10^{15}$
2	2023-02-23(16:07) to 02-24(02:07)	Flux decrease	$-5.0 \times 10^{15}$	$-8.5 \times 10^{15}$	–
3	2023-02-24(02:07) to 02-24(22:07)	Negative flux decrease	$+5.4 \times 10^{14}$	$-2.6 \times 10^{15}$	–
4	2023-02-24(22:07) to 02-25(13:07)	Slow Change in flux	$-9.6 \times 10^{14}$	$+2.4 \times 10^{14}$	–

**Table 3** Variation of average horizontal velocities in different stages and in different regions R1, R2, R3, R4.

Region	Stage-I $v_x$ ( $\text{m s}^{-1}$ )	Stage-II $v_x$ ( $\text{m s}^{-1}$ )	Stage-III $v_x$ ( $\text{m s}^{-1}$ )	Stage-IV $v_x$ ( $\text{m s}^{-1}$ )
R1	$10 \pm 9$	$10 \pm 14$	$7 \pm 12$	$0 \pm 18$
R2	$-39 \pm 27$	$-24 \pm 20$	$-15 \pm 11$	$-8 \pm 11$
R3	$11 \pm 27$	$23 \pm 27$	$24 \pm 22$	$13 \pm 16$
R4	$-34 \pm 29$	$-16 \pm 21$	$-12 \pm 32$	$-9 \pm 28$

magnetogram, which was taken at 00:10 UT on 2023 February 22. The horizontal velocity averaged over 00:10 UT on 2023 February 22 and 05:58 UT on 2023 February 23 is superimposed on them, which is obtained by the LCT method with respect to HMI longitudinal magnetograms. Usually, the characteristics of flows in and around the sunspot were revealed by Denker and Verma (2011). We focused on the four regions marked with white rectangles in Figure 5. The averaged velocity in the  $x$ -direction in four stages is listed in Table 3.

We have seen in stage-I that the horizontal flows are more divergent and less turbulent (i.e., less spread or irregular due to stronger flow initially) in region R2 as shown in Figure 5.

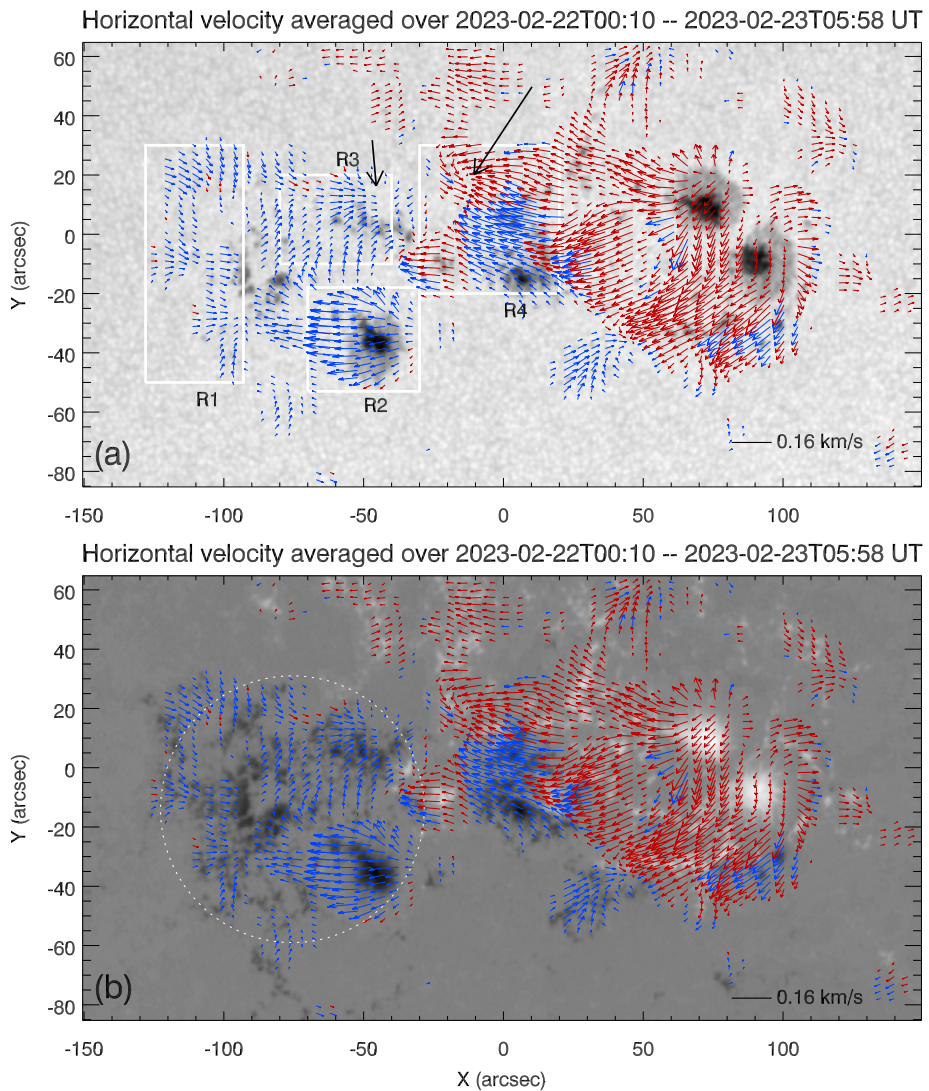


**Figure 5** Evolution of horizontal flows over time in stage I. Panel (a) shows the HMI continuum on which horizontal velocity flow patterns (averaged over 00:10 UT on 2023 February 22 and 05:58 UT on 2023 February 23) are superimposed. Panel (b) represents the HMI radial magnetogram on which horizontal velocity flow patterns (averaged over 00:10 UT on 2023 February 22 and 05:58 UT on 2023 February 23) are superimposed. The map has the field of view of  $300 \text{ arcsec} \times 150 \text{ arcsec}$ .

The bulk flow in region R2 was relatively stronger towards the east, but it met a reverse weak flow from that in region R1. This flow also moved up towards region R3 in the  $y$ -direction, but the flow of region R3 met a strong flow from R4. It seems that the flow in region R2 was tightly constricted by the flows from regions R1, R3, and R4. The sunspot S1 in region R2 shows a fast decay in the area at first due to more divergent flows, but the dominant negative flux decreased very slowly due to less turbulence in horizontal flows, likely as the diffused flux cannot escape freely in this region and only the magnetic cancellation in this

region annihilated the negative flux. Hence, initially, the flow in region R2 is fast and erodes the sunspot S1 rapidly, and its area decay is fast at the initial stage. The bulk flow in region R4, located in the polarity inversion region (also the position of S2), moved towards the east and was constricted by the westward flow of region R3. The negative flux cancelled with the positive fluxes from its east, west, and northward directions. Therefore, its area and magnetic fluxes of both polarity decreased rapidly. There is also a convergence of horizontal flows (see black arrows) within and very close to regions R3 and R4 (see Figure 5).

It is found in stage II (see Figure 6) that there were two obvious changes in the bulk flow in regions R2–R4. One is that the flow velocity in region R2 decreased from  $-39$  to  $-24 \text{ m s}^{-1}$  shown in Table 3. This suggests that the velocity of magnetic diffusion declined. Second is that the flow in region R3 became strong (from  $11$  to  $23 \text{ m s}^{-1}$ ) because it faced fewer opposing flows from region R4, and that in region R4 became weak (from  $34$  to  $16 \text{ m s}^{-1}$ ) because flows from regions (R1, R2, and R4) were added in region R3 whereas some flow in region R4 was left out and some faced opposite flows. At this stage, horizontal flows became more turbulent (more spreader or irregular flow) and less divergent. So, it verified the more negative flux decay and fewer sunspot area decay. We can also see the convergence of horizontal flows (see black arrows) within and very near to regions R3 and R4 (see Figure 6).

We plotted a circle that nearly encircles the regions of R1–R3 and superimposed it in Figure 6(b). We plotted the same circle and superimposed it in Figure 5(b). Obviously, by comparison, we noticed that the whole flow field shape of regions R1–R3 is converted into a nearly round shape in this stage, but that stage shows an oval shape and the long axis was roughly in the  $135^\circ$  direction ( $0^\circ$  in the  $x$ -direction). It may be caused by a large compression from the flows of regions R2 and R4 (i.e., flows became less divergent and more turbulent). But now, their flow velocity has decreased. If there was a columnar magnetic flux located in the region of R1–R3, it was in a stable or balanced state. The magnetic diffusion temporally stopped and there was weak magnetic cancellation. In other words, magnetic pressure was balanced from all sides due to a lack of magnetic diffusion. There was no mass interchange between regions R3 and R4 due to the compressed balance. There was nearly no magnetic diffusion in this stage. This may reflect the fact that the magnetic diffusion of the sunspot S1 became saturated temporally. The magnetic cancellation continued and both fluxes in the sunspot S2 continued to decrease.

It is seen in stage III (see Figure 7) that the flow velocities decrease in regions R1, R2, and R4, except for region R3. Now, horizontal flows can be classified as more turbulent and chaotic (i.e., irregular or more spread flow because of decreased magnetic flux). The average velocity in region R3 was  $24 \text{ m s}^{-1}$ , which is larger than that in region R4. There was a flow in region R3 moving to region R4. We can say that the mass flow of continuity is followed in region R3 in this stage, i.e., the outflow is nearly equal to the inflow ( $23$  to  $24 \text{ m s}^{-1}$ ) that is why its velocity remains almost same. There was also the field diffused out of the circle mainly on its east side (see Figure 7(b)). As the field moved outside of region R1, the field compression may have decreased due to the least divergence of flows (i.e., the magnetic pressure exerted by flows from region R1 on region R2 is decreased because some flows leaked from the south and east side. So, magnetic pressure is not balanced from all sides due to the lack of magnetic pressure exerted by region R1). The sunspot S2 decayed with a larger amplitude ( $1.8 \times 10^9 \text{ m}^2 \text{ s}^{-1}$ ) than that ( $5.6 \times 10^8 \text{ m}^2 \text{ s}^{-1}$ ) in the first stage (see Table 1). The magnetic flux began to decrease rapidly due to both the magnetic cancellation and the field escaping from the region R1 (i.e., less addition of flows in region R3 and lack of convergence of flows seen in Figure 7). As a result, flows were escaping (from the west side) rapidly from region R3 because it did not face any opposition and convergence. This can be a reason for the faster decay rate of sunspot S2 in this stage compared with stage I.

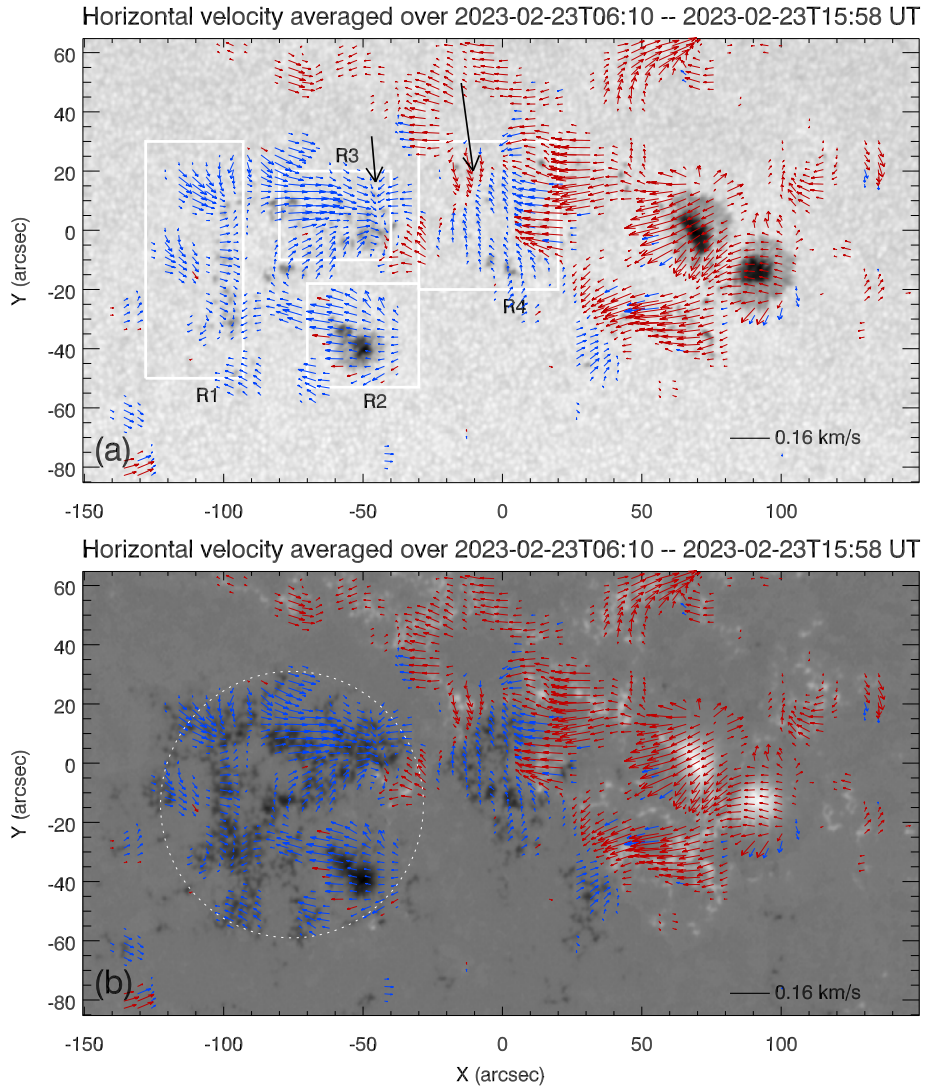


**Figure 6** Evolution of horizontal flows over time in stage II. Panel (a) shows the HMI continuum on which horizontal velocity flow patterns (averaged over 06:10 UT on 2023 February 23 and 15:58 UT on 2023 February 23) are superimposed. Panel (b) represents the HMI radial magnetogram on which horizontal velocity flow patterns (averaged over 06:10 UT of 2023 February 23 and 15:58 UT on 2023 February 23) are superimposed. The map has the field of view of  $300 \text{ arcsec} \times 150 \text{ arcsec}$ .

It is noticed in stage IV (see Figure 8) that the flow fields in regions R1 to R4 all continued to decrease with large amplitude and now flows were very weak and disorganized. The average field velocity in region R1 was zero. The flow field divided into two parts (in region R1), one moved towards the east and the other towards the west. There were more fluxes moved out of the circle from its east side (see Figure 8(b)), and a continuous flux flow was formed located on its south side. The positive flux completely disappeared in this stage. The decay of the sunspot S1 decreased to  $2.8 \times 10^6 \text{ m}^2 \text{ s}^{-1}$ , but the rate of flux decrease

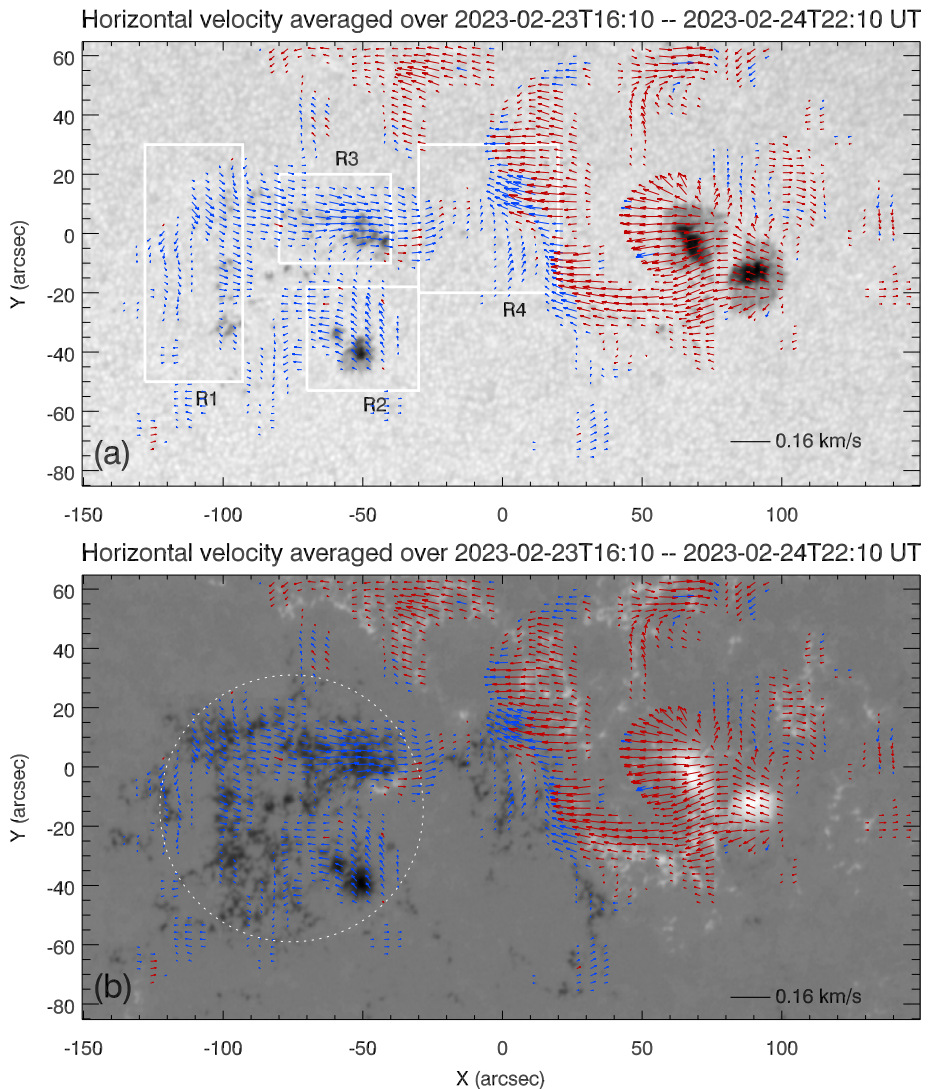


**Figure 7** Evolution of horizontal flows over time in stage III. Panel (a) shows the HMI continuum on which horizontal velocity flow patterns (averaged over 16:10 UT of 2023 February 23 and 22:10 UT of 2023 February 24) are superimposed. Panel (b) represents the HMI radial magnetogram on which horizontal velocity flow patterns (averaged over 16:10 UT of 2023 February 23 and 22:10 UT of 2023 February 24) are superimposed. The map has the field of view of  $300 \text{ arcsec} \times 150 \text{ arcsec}$ .

was similar to the last stage. At the last stage, the flow speeds became weaker so the sunspot decay rates decreased because the erosion of sunspots became smaller. In addition, the net horizontal flows in region R4 (sunspot S2 location) was zero because sunspot S2 had completely disappeared. The sunspot decay can also be verified by horizontal flows. It has been found that horizontal flows play a key role in the decay of sunspots via erosion, magnetic diffusion, and fragmentation.

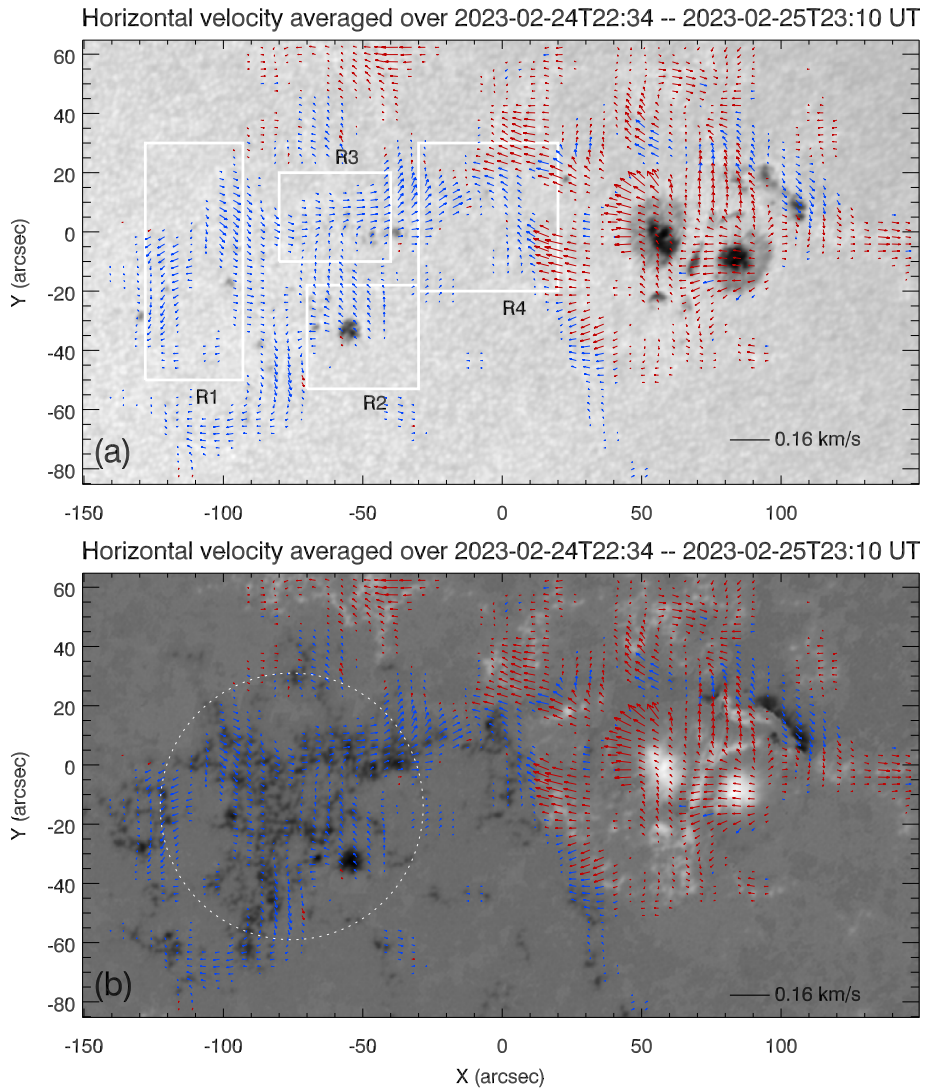


**Figure 8** Evolution of horizontal flows over time in stage IV. Panel (a) shows the HMI continuum on which horizontal velocity flow patterns (averaged over 22:34 UT of 2023 February 24 and 23:10 UT of 2023 February 25) are superimposed. Panel (b) represents the HMI radial magnetogram on which horizontal velocity flow patterns (averaged over 22:34 UT of 2023 February 24 and 23:10 UT of 2023 February 25) are superimposed. The map has the field of view of  $300 \text{ arcsec} \times 150 \text{ arcsec}$ .

As a result of these flows, the reconnection of the magnetic fields near the magnetic polarity inversion line may lead to the submergence of the surrounding magnetic field to the magnetic polarity inversion line which is the direct cause of the rapid attenuation of sunspot S1. Moreover, the convergence of horizontal flows may also have a relation to the sunspot decay because the convergence phenomenon is dominant initially and sunspot decay (area and especially magnetic flux) is also fast at the start. The maximum magnetic diffusivity

( $\eta_m$ ) of sunspots was calculated as  $\eta_m = 1.8 \times 10^9 \text{ m}^2 \text{ s}^{-1}$ . It was higher than the normal magnetic diffusivity ( $\eta_m = 10^4 \text{ m}^2 \text{ s}^{-1}$ ).

#### 4. Conclusion and Discussion

In this study, an investigation of the decay of  $\beta$ -type sunspots in the specified AR NOAA 13229 has been done. We utilized the data collected by ASO-S/FMG and SDO/HMI. In this research paper, area decay, magnetic dispersion of distinct sunspots, and the key mechanisms that played an important role in sunspot decay have been focused on. There are the following results:

(1) We found five processes responsible for sunspot decay known as convergence of horizontal flows, rotation of horizontal flows, fragmentation, magnetic diffusion and magnetic cancellation, and evidence for the existence of submergence of magnetic flux. It has been noticed that magnetic cancellation is more prominent in the decay of sunspot S2 whereas the fragmentation and magnetic diffusion played significant roles in the decay of sunspot S1. The area decay rate of the sunspot S1 varied from  $5.6 \times 10^8$  to  $2.8 \times 10^6 \text{ m}^2 \text{ s}^{-1}$ . Meanwhile, the decay rate of sunspot S2 remained  $1.9 \times 10^{15} \text{ m}^2 \text{ s}^{-1}$ . The calculated value of magnetic diffusivity was  $1.8 \times 10^9 \text{ m}^2 \text{ s}^{-1}$  which is an anomalous magnetic diffusion (normal  $\sim 10^4 \text{ m}^2 \text{ s}^{-1}$ ).

(2) The sunspots S1 and S2 had different decay rates and magnetic features. The decay rate of sunspot S2 was faster than that of sunspot S1 and they followed the exponential and parabolic decay laws, respectively. In parabolic decay, the initial decay rate is faster than in later stages and it obeys descending order. The sunspot S2 disappeared completely in 35 hours from 05:07 UT on 2023 February 22 to 11:07 UT on 2023 February 23.

(3) The positive flux of sunspot S1 was negligible and its negative flux decreased very slowly (slightly change) at the start for up to 50 hours and then declined linearly. On the other hand, the negative magnetic flux ( $2.4 \times 10^{21} \text{ Mx}$ ) of sunspot S2 was greater than its positive magnetic flux ( $1.3 \times 10^{21} \text{ Mx}$ ). Both declined with the same pattern (same rate), showing the magnetic cancellation process.

(4) The flow maps (horizontal velocities flows) obtained using the LCT technique revealed the key role of the horizontal flows in the area decay and magnetic flux diminished characteristics of sunspots. It has been found that the horizontal velocities are decreased with the decay of sunspots. The decreased trend of horizontal velocities was observed from  $-39$  to  $-8 \text{ m s}^{-1}$  and from  $-34$  to  $-9 \text{ m s}^{-1}$  in regions R2 (sunspot S1) and R4 (sunspot S2), respectively. We also found the convergence of horizontal flows initially in the first two stages where the decay process and horizontal velocities flows were fast.

(5) At the start, more divergent (i.e., carrying material away from the center of the sunspot) and less turbulent flows (i.e., breaking up the sunspots) have been observed. In the middle stage, flows became more turbulent and less divergent. In the last stage, flows converted into being more turbulent and chaotic. It revealed the fact that divergence of flows plays a significant role in the area decay, and the turbulence of flows plays a prominent role in magnetic diffusion of sunspots.

(6) The evidence for the existence of an important mechanism has been found which is known as the submergence of magnetic fluxes, which is also a key reason for the sunspot decay.

Previously, a simulation-based study has revealed that the process of submergence of magnetic fluxes plays an important role in the decay of sunspots (Rempel, 2015) but it has not been verified by observational studies. In this study, we observed the submergence of



magnetic flux in the middle of regions R3 and R4 which played a significant role in the sunspot decay. Our detailed case study of a specific active region contributes to the overall understanding of sunspot dynamics. We observed processes like magnetic cancellation, fragmentation, and, crucially, submergence, which support findings by Howard (1992), Norton et al. (2017), Muraközy (2021, 2022). By integrating these mechanisms with established models, we highlight the complexity of sunspot evolution, where spatial positioning and magnetic field dynamics within active regions play a critical role.

Previous studies suggested that the area decay of sunspots is either a linear (Solanki, 2003; Li et al., 2021) or quadratic (Litvinenko and Wheatland, 2015) function of time. Most of the research showed the linear area decay of different sunspots. The area growth rates of 399 sunspot groups have been investigated by using the solar and Heliospheric Observatory/Michelson Doppler Imager–Derecen Data (SDD) sunspot catalogue and discovered that an asymmetric Gaussian function well suited the sunspot groups' growth and decay processes (Muraközy, Baranyi, and Ludmány, 2014). Our results expressed different decay rates and magnetic features of two sunspots S1 and S2. One of our interesting findings is the exponential decay of sunspot S2 and its complete disappearance within a short time. On the other hand, the sunspot S1 decay pattern showed different rates during the four stages of its decay, and it remained as a pore at the end.

According to some study results, the magnetic flux diminishes linearly as the sunspot decays (Verma et al., 2016; Deng et al., 2007; Li et al., 2021). This is not justified by our results. In our case, magnetic flux decreased in different stages. The positive flux of sunspot S1 remained almost constant but its negative flux varied in two steps. Initially, it decreased slightly and, in the second stage, it declined linearly. On the other hand, the diminishing trend of the negative and positive fluxes of sunspot S2 is nearly the same, but their declining patterns were also not purely linear. They decreased in descending rate steps. Moreover, the flux decay of the sunspot not only happened on its edges but throughout the sunspot. The turbulent diffusion model follows these findings (Solanki, 2003; Meyer et al., 1974; Martínez Pillet, 2002). The negative magnetic flux of sunspot S1 decline rate varied from  $-2.0 \times 10^{14}$  to  $-2.3 \times 10^{16}$  Mx. On the other hand, positive and negative magnetic fluxes of sunspot S2 changed from  $-5.0 \times 10^{15}$  to  $-9.6 \times 10^{14}$  Mx and from  $-8.5 \times 10^{15}$  to  $2.4 \times 10^{14}$  Mx, respectively. There will be a lot of MMFs pouring out of the sunspot throughout the destruction phase. MMFs may be responsible for the sunspot's magnetic flux decline. A previous study suggests that during sunspot decline, the magnetic flux in the sunspot is transmitted via MMFs to the surrounding network (Verma and Denker, 2012; Deng et al., 2007). It is also suggested by some researchers that an extension of Evershed flows is considered MMFs (Cabrera Solana et al., 2006).

**Acknowledgments** Thanks to the referee's constructive comments and suggestions, the manuscript has undergone significant improvements. This research was supported by the National Key R & D Program of China (Nos. 2022YFF0503001, 2021YFA1600500, and 2022YFF0503800), the Strategic Priority Research Program of the Chinese Academy of Sciences (Grant NO. XDB0560301), the National Natural Science Foundation of China (grant Nos. 12273059 and 12373057) and the Beijing Natural Science Foundation (Grant No. 1222029). We would like to thank the ASO-S and SDO/HMI teams for providing the data on the NOAA AR 13229, and the ANSO funding organization for supporting author's doctoral study.

**Author contributions** All authors contributed and reviewed the manuscript.

**Data Availability** The datasets used in this study were obtained from publicly available sources: SDO/HMI data from JSOC Lookdata (JSOC Lookdata, Stanford University) and ASOS/FMG data from the ASOS Data Center (ASOS Data Archive).

## Declarations

**Competing interests** The authors declare no competing interests.

## References

- Bellot Rubio, L.R., Tritschler, A., Martínez Pillet, V.: 2008, Spectropolarimetry of a decaying sunspot penumbra. *Astrophys. J.* **676**, 698. DOI. ADS.
- Bumba, V.: 1963, Development of SPOT group areas in dependence on the local magnetic field. *Bull. Astron. Inst. Czechoslov.* **14**, 91. ADS.
- Cabrera Solana, D., Bellot Rubio, L.R., Beck, C., del Toro Iniesta, J.C.: 2006, Evershed clouds as precursors of moving magnetic features around sunspots. *Astrophys. J. Lett.* **649**, L41. DOI. ADS.
- Chae, J.: 2001, Observational determination of the rate of magnetic helicity transport through the solar surface via the horizontal motion of field line footpoints. *Astrophys. J. Lett.* **560**, L95. DOI. ADS.
- Chapman, G.A., Dobias, J.J., Preminger, D.G., Walton, S.R.: 2003, On the decay rate of sunspots. *Geophys. Res. Lett.* **30**, 1178. DOI. ADS.
- Chen, J., Su, J., Yin, Z., Priya, T.G., Zhang, H., Liu, J., Xu, H., Yu, S.: 2015, Recurrent solar jets induced by a satellite spot and moving magnetic features. *Astrophys. J.* **815**, 71. DOI. ADS.
- Démoulin, P., Berger, M.A.: 2003, Magnetic energy and helicity fluxes at the photospheric level. *Solar Phys.* **215**, 203. DOI. ADS.
- Deng, N., Liu, C., Yang, G., Wang, H., Denker, C.: 2005, Rapid penumbral decay associated with an X2.3 flare in NOAA active region 9026. *Astrophys. J.* **623**, 1195. DOI. ADS.
- Deng, N., Choudhary, D.P., Tritschler, A., Denker, C., Liu, C., Wang, H.: 2007, Flow field evolution of a decaying sunspot. *Astrophys. J.* **671**, 1013. DOI. ADS.
- Deng, Y.-Y., Zhang, H.-Y., Yang, J.-F., Li, F., Lin, J.-B., Hou, J.-F., Wu, Z., Song, Q., Duan, W., Bai, X.-Y., Wang, D.-G., Lv, J., Ge, W., Wang, J.-N., Zheng, Z.-Y., Wang, C.-J., Wang, N.-G., Ni, H.-K., Zeng, Y.-Z., Zhang, Y., Yang, X., Sun, Y.-Z., Zhang, Z.-Y., Wang, X.-F.: 2019, Design of the Full-disk Magnetograph (FMG) onboard the ASO-S. *Res. Astron. Astrophys.* **19**, 157. DOI. ADS.
- Denker, C., Verma, M.: 2011, Velocity fields in and around sunspots at the highest resolution. In: Prasad Choudhary, D., Strassmeier, K.G. (eds.) *Physics of Sun and Star Spots* **273**, 204. DOI. ADS.
- Gafeira, R., Fonte, C.C., Pais, M.A., Fernandes, J.: 2014, Temporal evolution of sunspot areas and estimation of related plasma flows. *Solar Phys.* **289**, 1531. DOI. ADS.
- Gan, W.-Q., Zhu, C., Deng, Y.-Y., Li, H., Su, Y., Zhang, H.-Y., Chen, B., Zhang, Z., Wu, J., Deng, L., Huang, Y., Yang, J.-F., Cui, J.-J., Chang, J., Wang, C., Wu, J., Yin, Z.-S., Chen, W., Fang, C., Yan, Y.-H., Lin, J., Xiong, W.-M., Chen, B., Bao, H.-C., Cao, C.-X., Bai, Y.-P., Wang, T., Chen, B.-L., Li, X.-Y., Zhang, Y., Feng, L., Su, J.-T., Li, Y., Chen, W., Li, Y.-P., Su, Y.-N., Wu, H.-Y., Gu, M., Huang, L., Tang, X.-J.: 2019, Advanced Space-based Solar Observatory (ASO-S): An overview. *Res. Astron. Astrophys.* **19**, 156. DOI. ADS.
- Gan, W., Zhu, C., Deng, Y., Zhang, Z., Chen, B., Huang, Y., Deng, L., Wu, H., Zhang, H., Li, H., Su, Y., Su, J., Feng, L., Wu, J., Cui, J., Wang, C., Chang, J., Yin, Z., Xiong, W., Chen, B., Yang, J., Li, F., Lin, J., Hou, J., Bai, X., Chen, D., Zhang, Y., Hu, Y., Liang, Y., Wang, J., Song, K., Guo, Q., He, L., Zhang, G., Wang, P., Bao, H., Cao, C., Bai, Y., Chen, B., He, T., Li, X., Zhang, Y., Liao, X., Jiang, H., Li, Y., Su, Y., Lei, S., Chen, W., Li, Y., Zhao, J., Li, J., Ge, Y., Zou, Z., Hu, T., Su, M., Ji, H., Gu, M., Zheng, Y., Xu, D., Wang, X.: 2023, The Advanced Space-based Solar Observatory (ASO-S). *Solar Phys.* **298**, 68. DOI. ADS.
- Hathaway, D.H., Choudhary, D.P.: 2008, Sunspot group decay. *Solar Phys.* **250**, 269. DOI. ADS.
- Hoeksema, J.T., HMI Project Team: 2007, *The Helioseismic & Magnetic Imager on the Solar Dynamics Observatory*. In: American Astronomical Society Meeting Abstracts **210**, 24.15. ADS.
- Hou, J.-F., Wang, D.-G., Deng, Y.-Y., Zhang, Z.-Y., Sun, Y.-Z.: 2020, Interference effect on the liquid-crystal-based Stokes polarimeter. *Chin. Phys. B* **29**, 124211.
- Howard, R.F.: 1992, Some characteristics of the development and decay of active region magnetic flux. *Solar Phys.* **142**, 47. DOI. ADS.
- Jiang, C., Feng, X.: 2013, Extrapolation of the solar coronal magnetic field from SDO/HMI magnetogram by a CESE-MHD-NLFFF code. *Astrophys. J.* **769**, 144. DOI. ADS.
- Krause, F., Ruediger, G.: 1975, On the turbulent decay of strong magnetic fields and the development of sunspot areas. *Solar Phys.* **42**, 107. DOI. ADS.
- Leka, K.D., Skumanich, A.: 1998, The evolution of pores and the development of penumbrae. *Astrophys. J.* **507**, 454. DOI. ADS.

- Li, Q., Yan, X., Wang, J., Kong, D., Xue, Z., Yang, L., Cao, W.: 2018, The formation of a sunspot penumbra sector in active region NOAA 12574. *Astrophys. J.* **857**, 21. DOI. ADS.
- Li, Q., Zhang, L., Yan, X., Wang, J., Kong, D., Yang, L., Xue, Z.: 2021, The decay of  $\alpha$ -configuration sunspots. *Astrophys. J.* **913**, 147. DOI. ADS.
- Lim, E.-K., Yurchyshyn, V., Goode, P., Cho, K.-S.: 2013, Observation of a non-radial penumbra in a flux emerging region under photospheric canopy fields. *Astrophys. J. Lett.* **769**, L18. DOI. ADS.
- Litvinenko, Y.E., Wheatland, M.S.: 2015, Modeling sunspot and starspot decay by turbulent erosion. *Astrophys. J.* **800**, 130. DOI. ADS.
- Liu, Y., Scherrer, P.H., Hoeksema, J.T., Schou, J., Bai, T., Beck, J.G., Bobra, M., Bogart, R.S., Bush, R.I., Couvidat, S., Hayashi, K., Kosovichev, A.G., Larson, T.P., Rabello-Soares, C., Sun, X., Wachter, R., Zhao, J., Zhao, X.P., Duvall, J.T.L., DeRosa, M.L., Schrijver, C.J., Title, A.M., Centeno, R., Tomczyk, S., Borrero, J.M., Norton, A.A., Barnes, G., Crouch, A.D., Leka, K.D., Abbott, W.P., Fisher, G.H., Welsch, B.T., Muglach, K., Schuck, P.W., Wiegmann, T., Turmon, M., Linker, J.A., Mikić, Z., Riley, P., Wu, S.T.: 2012, A first look at magnetic field data products from SDO/HMI. In: Bellot Rubio, L., Reale, F., Carlsson, M. (eds.) *4th Hinode Science Meeting: Unsolved Problems and Recent Insights*, *Astronomical Society of the Pacific Conference Series* **455**, 337. ADS.
- MacTaggart, D., Guglielmino, S.L., Zuccarello, F.: 2016, The pre-penumbra magnetic canopy in the solar atmosphere. *Astrophys. J. Lett.* **831**, L4. DOI. ADS.
- Martínez Pillet, V.: 2002, Decay of sunspots. *Astron. Nachr.* **323**, 342. [https://doi.org/10.1002/1521-3994\(200208\)323:3/4<342::AID-ASNA342>3.0.CO;2-5](https://doi.org/10.1002/1521-3994(200208)323:3/4<342::AID-ASNA342>3.0.CO;2-5). ADS.
- Martínez Pillet, V., Moreno-Insertis, F., Vazquez, M.: 1993, The distribution of sunspot decay rates. *Astron. Astrophys.* **274**, 521. ADS.
- Meyer, F., Schmidt, H.U., Weiss, N.O., Wilson, P.R.: 1974, The growth and decay of sunspots. *Mon. Not. Roy. Astron. Soc.* **169**, 35. DOI. ADS.
- Murabito, M., Romano, P., Guglielmino, S.L., Zuccarello, F., Solanki, S.K.: 2016, Formation of the penumbra and start of the Evershed flow. *Astrophys. J.* **825**, 75. DOI. ADS.
- Muraközy, J.: 2020, Study of the decay rates of the umbral area of sunspot groups using a high-resolution database. *Astrophys. J.* **892**, 107. DOI. ADS.
- Muraközy, J.: 2021, On the decay of sunspot groups and their internal parts in detail. *Astrophys. J.* **908**, 133. DOI. ADS.
- Muraközy, J.: 2022, Variations of the internal asymmetries of sunspot groups during their decay. *Astrophys. J.* **925**, 87. DOI. ADS.
- Muraközy, J., Baranyi, T., Ludmány, A.: 2014, Sunspot group development in high temporal resolution. *Solar Phys.* **289**, 563. DOI. ADS.
- Norton, A.A., Jones, E.H., Linton, M.G., Leake, J.E.: 2017, Magnetic flux emergence and decay rates for pre- and follower sunspots observed with HMI. *Astrophys. J.* **842**, 3. DOI. ADS.
- November, L.J., Simon, G.W.: 1988, Precise proper-motion measurement of solar granulation. *Astrophys. J.* **333**, 427. DOI. ADS.
- Petrovay, K., Martínez Pillet, V., van Driel-Gesztelyi, L.: 1999, Making sense of sunspot decay – II. Deviations from the mean law and plage effects. *Solar Phys.* **188**, 315. DOI. ADS.
- Petrovay, K., Moreno-Insertis, F.: 1997, Turbulent erosion of magnetic flux tubes. *Astrophys. J.* **485**, 398. DOI. ADS.
- Petrovay, K., van Driel-Gesztelyi, L.: 1997, Making sense of sunspot decay. I. Parabolic decay law and Gnevyshev-Waldmeier relation. *Solar Phys.* **176**, 249. DOI. ADS.
- Rempel, M.: 2011, Penumbra fine structure and driving mechanisms of large-scale flows in simulated sunspots. *Astrophys. J.* **729**, 5. DOI. ADS.
- Rempel, M.: 2012, Numerical sunspot models: robustness of photospheric velocity and magnetic field structure. *Astrophys. J.* **750**, 62. DOI. ADS.
- Rempel, M.: 2015, Numerical simulations of sunspot decay: on the penumbra-Evershed flow-moat flow connection. *Astrophys. J.* **814**, 125. DOI. ADS.
- Romano, P., Guglielmino, S.L., Cristaldi, A., Ermolli, I., Falco, M., Zuccarello, F.: 2014, Evolution of the magnetic field inclination in a forming penumbra. *Astrophys. J.* **784**, 10. DOI. ADS.
- Romano, P., Murabito, M., Guglielmino, S.L., Zuccarello, F., Falco, M.: 2020, Restoring process of sunspot penumbra. *Astrophys. J.* **899**, 129. DOI. ADS.
- Rüdiger, G., Kitchatinov, L.L.: 2000, Sunspot decay as a test of the eta-quenching concept. *Astron. Nachr.* **321**, 75. [https://doi.org/10.1002/\(SICI\)1521-3994\(200003\)321:1<75::AID-ASNA75>3.0.CO;2-B](https://doi.org/10.1002/(SICI)1521-3994(200003)321:1<75::AID-ASNA75>3.0.CO;2-B). ADS.
- Sainz Dalda, A., Martínez Pillet, V.: 2005, Moving magnetic features as prolongation of penumbral filaments. *Astrophys. J.* **632**, 1176. DOI. ADS.
- Scherrer, P.H., Schou, J., Bush, R.I., Kosovichev, A.G., Bogart, R.S., Hoeksema, J.T., Liu, Y., Duvall, T.L., Zhao, J., Title, A.M., Schrijver, C.J., Tarbell, T.D., Tomczyk, S.: 2012, The Helioseismic and Magnetic

- Imager (HMI) investigation for the Solar Dynamics Observatory (SDO). *Solar Phys.* **275**, 207. DOI. ADS.
- Schlichenmaier, R., Rezaei, R., Bello González, N., Waldmann, T.A.: 2010, The formation of a sunspot penumbra. *Astron. Astrophys.* **512**, L1. DOI. ADS.
- Schou, J., Scherrer, P.H., Bush, R.I., Wachter, R., Couvidat, S., Rabello-Soares, M.C., Bogart, R.S., Hoeksema, J.T., Liu, Y., Duvall, T.L., Akin, D.J., Allard, B.A., Miles, J.W., Rairden, R., Shine, R.A., Tarbell, T.D., Title, A.M., Wolfson, C.J., Elmore, D.F., Norton, A.A., Tomczyk, S.: 2012, Design and ground calibration of the Helioseismic and Magnetic Imager (HMI) instrument on the Solar Dynamics Observatory (SDO). *Solar Phys.* **275**, 229. DOI. ADS.
- Sheeley, J.N.R., Stauffer, J.R., Thomassie, J.C., Warren, H.P.: 2017, Tracking the magnetic flux in and around sunspots. *Astrophys. J.* **836**, 144. DOI. ADS.
- Shimizu, T., Ichimoto, K., Suematsu, Y.: 2012, Precursor of sunspot penumbral formation discovered with hinode solar optical telescope observations. *Astrophys. J. Lett.* **747**, L18. DOI. ADS.
- Skumanich, A., Lites, B.W.: 1994, Vector field structure of a small sunspot. In: Schüssler, M., Schmidt, W. (eds.) *Solar Magnetic Fields*, 200. ADS.
- Solanki, S.K.: 2003, Sunspots: An overview. *Astron. Astrophys. Rev.* **11**, 153. DOI. ADS.
- Strecker, H., Bello González, N.: 2018, Evolution of the flow field in decaying active regions. Transition from a moat flow to a supergranular flow. *Astron. Astrophys.* **620**, A122. DOI. ADS.
- Su, J.-T., Bai, X.-Y., Chen, J., Guo, J.-J., Liu, S., Wang, X.-F., Xu, H.-Q., Yang, X., Song, Y.-L., Deng, Y.-Y., Ji, K.-F., Deng, L., Huang, Y., Li, H., Gan, W.-Q.: 2019, Data reduction and calibration of the FMG onboard ASO-S. *Res. Astron. Astrophys.* **19**, 161. DOI. ADS.
- Thomas, J.H., Weiss, N.O., Tobias, S.M., Brummell, N.H.: 2002, Downward pumping of magnetic flux as the cause of filamentary structures in sunspot penumbrae. *Nature* **420**, 390. DOI. ADS.
- Verma, M., Denker, C.: 2012, Horizontal flow fields observed in Hinode G-band images. III. The decay of a satellite sunspot and the role of magnetic flux removal in flaring. *Astron. Astrophys.* **545**, A92. DOI. ADS.
- Verma, M., Denker, C., Balthasar, H., Kuckein, C., González Manrique, S.J., Sobotka, M., Bello González, N., Hoch, S., Diercke, A., Kummerow, P., Berkefeld, T., Collados, M., Feller, A., Hofmann, A., Kneer, F., Lagg, A., Löhner-Böttcher, J., Nicklas, H., Pastor Yabar, A., Schlichenmaier, R., Schmidt, D., Schmidt, W., Schubert, M., Sigwarth, M., Solanki, S.K., Soltau, D., Staude, J., Strassmeier, K.G., Volkmer, R., von der Lühe, O., Waldmann, T.: 2016, Horizontal flow fields in and around a small active region. The transition period between flux emergence and decay. *Astron. Astrophys.* **596**, A3. DOI. ADS.
- Verma, M., Denker, C., Balthasar, H., Kuckein, C., Rezaei, R., Sobotka, M., Deng, N., Wang, H., Tritschler, A., Collados, M., Diercke, A., González Manrique, S.J.: 2018, High-resolution imaging and near-infrared spectroscopy of penumbral decay. *Astron. Astrophys.* **614**, A2. DOI. ADS.
- Wang, H., Liu, C., Qiu, J., Deng, N., Goode, P.R., Denker, C.: 2004, Rapid penumbral decay following three X-class solar flares. *Astrophys. J. Lett.* **601**, L195. DOI. ADS.
- Watanabe, H., Kitai, R., Otsuji, K.: 2014, Formation and decay of rudimentary penumbra around a pore. *Astrophys. J.* **796**, 77. DOI. ADS.

**Publisher's Note** Springer Nature remains neutral with regard to jurisdictional claims in published maps and institutional affiliations.

Springer Nature or its licensor (e.g. a society or other partner) holds exclusive rights to this article under a publishing agreement with the author(s) or other rightsholder(s); author self-archiving of the accepted manuscript version of this article is solely governed by the terms of such publishing agreement and applicable law.